Available online at www.sciencedirect.com
ScienceDirect
Remote Sensing of Environment 112 (2008) 2850–2862
Remote Sensing of Environment
www.elsevier.com/locate/rse

Continuous wavelets for the improved use of spectral libraries and hyperspectral data

B. Rivard *, J. Feng, A. Gallie, A. Sanchez-Azofeifa

Earth Observation Systems Laboratory, Department of Earth and Atmospheric Sciences, University of Alberta, Edmonton, Alberta, Canada T6G 2E3

Received 5 October 2007; received in revised form 24 January 2008; accepted 26 January 2008

Abstract

Spectral libraries are commonly established as a means to archive representative signatures of natural materials. Such signatures can then be used to train feature extraction and classification algorithms applied to imagery, for comparison with unlabeled spectra. A number of spectral libraries are publicly available and widely used in the community. Disparities in viewing and illumination measurement configurations between libraries generally preclude the direct comparison of spectra for the same materials. Within libraries, measurements may be reported for varying sample properties, such as grain size in the case of powdered minerals or leaf or canopy structure in the case of vegetation. In such instances, use of the library and the selection of representative spectra to identify an unknown material may require a priori knowledge or an educated guess of the physical properties of the unknown material to conduct the comparison.

This study demonstrates that continuous wavelet analysis can provide a new and useful representation of spectral libraries and minimize these disparities amongst libraries. In the context of spectral mixture analysis we suggest that the selection of representative endmember spectra from spectral libraries can be more readily defined in the wavelet domain than using reflectance data. In the context of sensing target compositional variability, for example changes in the chemistry of a given mineral, spectral differences due to distinct sample composition are more readily identified using wavelets. The examples provided in this paper are mainly for powdered mineral spectra because there are a number of widely known public spectral libraries of powdered minerals that have been in common use in the hyperspectral community but the principles apply to a range of natural materials including vegetation.

Keywords: Wavelet; Hyperspectral; Mineral; Unmixing; Spectral libraries

1. Introduction

Spectral libraries collected in the field and laboratory are common data sets exploited by the hyperspectral remote sensing community. Such data support the analysis of airborne and spaceborne hyperspectral imagery, the characterization of natural materials, and the development of algorithms for information extraction. The widespread availability of field portable spectroradiometers attests to the importance of such measurements for remote sensing investigations of the environment.

Spectral libraries are commonly established as a means to archive representative signatures of natural materials. Such signatures can then be used to train feature extraction and classification algorithms applied to imagery, for comparison with unlabeled spectra, and to define spectral endmembers as inputs for spectral unmixing. A number of spectral libraries are publicly available and widely used in the community, some are packaged with hyperspectral image-processing software (e.g. ENVI). Disparities in viewing and illumination measurement configurations between libraries generally preclude the direct comparison of spectra for the same materials. Within libraries, measurements may be reported for varying sample properties, such as grain size in the case of powdered minerals or leaf or canopy structure in the case of vegetation. In such instances, use of the library and the selection of representative spectra to

* Corresponding author. Tel.: +1 780 492 1822; fax: +1 780 492 2030.
E-mail address: benoit.rivard@ualberta.ca (B. Rivard).

0034-4257/$ - see front matter © 2008 Elsevier Inc. All rights reserved.
doi:10.1016/j.rse.2008.01.016

identify an unknown material may require a priori knowledge or an educated guess of the physical properties of the unknown material to conduct the comparison.

Each spectrum in a library exhibits a particular albedo, background continuum, and absorption features. For minerals, the location of absorption features is controlled by their chemical composition. The continuum and overall albedo are influenced by non-selective absorption and scattering, influenced by the physical (particle size, roughness, etc.) and chemical properties of the surface (Clark, 1999; Clark & Roush, 1984; Mustard & Sunshine, 1999) and the viewing and illumination geometry of the measurement. Given that these factors are not wavelength specific they are hereafter referred to as non-compositional effects. Differences in the non-compositional effects between samples of the same material can limit the usefulness of library spectra. A common practice to minimize the non-compositional effects involves isolating the spectral features (e.g. absorptions) from the background continuum (Clark, 1999; Clark et al., 2003; Mustard, 1992; Sunshine et al., 1990). Removal of the continuum also has the merit of providing the correct band center locations for absorption features extracted from a sloping continuum.

There are several problems with continuum removal, however. For one, the appropriate shape of the continuum is not always known, and different researchers use a constant, linear or curved baseline, fit either locally or to the entire spectrum (Clark, 1999; Sunshine & Pieters, 1993). For another, continuum removal is usually done by ratioing the continuum and the spectrum, a process which is non-linear and which results in continuum-removed spectra that cannot serve as inputs for linear spectral unmixing (LSU). LSU is one of the most commonly used analysis tools for hyperspectral imagery, and non-linear continuum removal limits the use of spectral libraries because library and imagery spectra must have the non-compositional background information removed in order to make them comparable. Such continuum-removed spectra can be used for comparison with unknown spectra for target identification and detection using tools such as spectral angle mapper (SAM, Kruse et al., 1993), spectral feature fitting (SFF, Clark et al., 1990; Clark & Swayze, 1995; Swayze & Clark, 1995) and Tetracorder (Clark et al., 2003). However, loss of the additive properties of continuum-removed spectra represents a significant problem. As an alternative, we propose to decompose a spectrum into linearly additive wavelets that isolate spectral features from their continuum over a broad spectral region. This process has the advantage that it removes the continuum for many spectral features in a single operation. Of equal significance, the fact that the wavelets are linearly additive implies that linear unmixing can be implemented in the wavelet domain.

In this study we show that continuous wavelet analysis can be used to provide a new representation of spectral libraries. We illustrate that disparities in measurement methodologies between libraries, and in variable sample physical properties between and within libraries, can be minimized. We then discuss the implications for the improved utilization of spectral libraries, specifically for determining spectral endmembers from libraries when multiple spectra for the same material are available. We pay particular attention to clay minerals because of their significance for mineral exploration. The examples provided in this paper are mainly for powdered mineral spectra because there are a number of widely known public spectral libraries of powdered minerals that have been in common use in the hyperspectral community but the principles apply to a range of natural materials including vegetation.

2. Description of spectral libraries and experiments

Abundant publicly available powdered mineral spectra were collected by the Jet Propulsion Laboratory (JPL, Grove et al., 1992, http://speclib.jpl.nasa.gov/documents/jpl_desc.htm), John Hopkins University (JHU, Salisbury et al., 1991, http://speclib.jpl.nasa.gov/documents/jhu_desc.htm), Arizona State University (ASU, Christensen et al., 2000, http://tes.asu.edu/spectral/library/index.html), and the United States Geological Survey (USGS, Clark et al., 1993, http://speclab.cr.usgs.gov/spectral.lib04/spectral-lib04.html) (Table 1). The mineralogy of the measured samples was characterized from a combination of analytical methods including X-ray diffraction, bulk chemistry from X-ray fluorescence and electron microprobe analysis (Table 1). The JPL and JHU libraries contain reflectance spectra and the ASU library contains emittance spectra (Ruff et al., 1997) which we converted to reflectance using Kirchoff's law (Hapke, 1993; Salisbury et al., 1994). The spectra from the JHU library are for bi-conical reflectance (Salisbury et al., 1991) at 10° of light incidence and viewing while the JPL spectra are for hemispherical reflectance. The 5–15 μm spectral range of measurement is common to all three data sets.

In a first experiment we aimed to facilitate comparison of spectra between different libraries. We wanted to minimize spectral differences introduced by the disparities in measurement methodologies amongst these libraries and differences in grain

Table 1
Data sets

Source	Spectral range (μm)	Spectral measurement	Particle sizes (um) [a]	Analytical method
John Hopkins University (JHU)	2.08–25.00	Bi-conical reflectance	0–75(F), 75–250 (C), solid (S), Packed powder[b]	XRD[1], XRF[1], Microprobe[1]
Jet Propulsion Laboratory (JPL)	2.00–15.39	Hemispherical reflectance	0–45 (F), 45–125 (M), 125–500 (C), solid (S), Packed powder	XRD[1], Microprobe[1]
Arizona State University (ASU)	5.00–45.45	Passive emittance (80 °C)	710–1000 (C), Solid (S)	XRD[1], Microprobe[1]
United States Geological Survey (USGS)	0.20–3.0	Bi-directional reflectance	Varies from sample to sample	XRD[2], XRF[2], Microprobe[2]

[a]F = fine; M = Medium; C = coarse; S = Solid; [b]For some minerals, fine powders were packed to simulate medium or coarse grain sizes; [1]Available for all samples; [2]Available for some samples. XRD: X-ray diffraction, XRF: X-ray fluorescence.

size between samples. For this purpose we chose to examine the spectra of the mineral quartz, one with a simple chemistry to minimize potential confounding effects introduced by compositional variability of samples resulting from variable geographical provenance. The selected quartz spectra are for a solid crystal (JHU) and powders of the following grain sizes: 75–250 μm (JHU), 45–125 μm (JPL), 125–500 μm (JPL) and 710–1000 μm (ASU).

In a second experiment we examined specifically if the spectral effects introduced by the variable grain size of the samples can be minimized. Therefore for each sample we examine multiple grain sizes collected with the same measurement set-up. The grain size of minerals is known to impact amplitude of the continuum and feature strength (Clark, 1999; Clark and Roush, 1984; Johnson et al., 1983, 1992; Hapke, 1993; Mustard & Hayes, 1997; Salisbury et al., 1991). Conel (1969), Hapke (1981), Johnson et al. (1983), Mustard and Pieterset (1989) and Ramsey and Christensen (1998) have attempted to quantitatively model mixtures of mineral powders of various particle sizes. The controls of grain size on mineral spectra are recognized as a challenge for the spectral analysis of laboratory and airborne/spaceborne data. For this experiment we focused on a subset of the JHU library encompassing 29 minerals at varying grain size (Table 2) for a total of 87 (29 * 3) spectra (fine grain 0–75 μm, coarse grain 75–250 μm and solid surface). The list of selected minerals includes common rock-forming minerals. When multiple samples were available for the same minerals, spectra from a single sample were selected to avoid compositional variability introduced by samples of variable geographical provenance. For some minerals (e.g. olivine), the JHU library contains spectra for packed fine powders (<75 μm) to emulate coarser powders (75–250 μm) that were not available. When fine powers are packed their spectra resembles that of larger particles (Adams & Filice, 1967; Pieters, 1983). The measured solid surfaces were natural fractures or cleavage surfaces (Salisbury et al., 1991). Together, these data capture high spectral variability observed for individual mineral samples as a function of grain size.

Most published investigations using spectral libraries are concerned with the visible short wave infrared (0.4–2.5 μm). Thus for the last experiment we examined spectra of all samples of 12 clay minerals from the USGS library (Table 3) and determined whether the selection of representative spectra of a given mineral can be facilitated by reduction of non-compositional effects using wavelets. These spectra are likely the most commonly used spectra in the geological community because of their relevance to the detection of rock alteration in remote sensing imagery (ASTER, Landsat) and their role in defining mining exploration targets.

3. Methodology

3.1. Continuous wavelets

Wavelet analysis is a signal-processing tool, which has been successfully used in meteorology (Farge, 1992; Meyers et al.,

Table 2
List of minerals and filename of spectra selected from the JHU library

Mineral Name	ID[a]	Composition	Sample Name [b]	Mineral group	Structure
Augite	1	$(CaNa)(MgFeAlTi)(SiAl)_2O_6$	augite.1	Pyroxene	Inosilicate
Enstatite	2	Mg_2Si2O_6	enstatite.1	Pyroxene	Inosilicate
Hedenbergite	3	$CaFeSi_2O_6$	hedenber.1	Pyroxene	Inosilicate
Hypersthene	4	$(MgFe)_2Si_2O_6$	hypersth.1	Pyroxene	Inosilicate
Jadeite	5	$Na(AlFe)Si_2O_6$	jadeite.1	Pyroxene	Inosilicate
Spodumene	6	$LiAlSi_2O_6$	olivine.12	Pyroxene	Inosilicate
Olivine (Fo_{92})	7	$(FeMg)_2SiO_4$	olivine.12	Olivine	Nesosilicate
Monticellite	8	$CaMgSiO_4$	monticell.1	Olivine	Nesosilicate
Richterite	9	$Na_2Ca(Mg\ Fe)_5Si_8O_{22}(OH)_2$	richter.1	Amphibole	Inosilicate
Riebeckite	10	$Na_2(FeMg)_3Fe_3Si_8O_{22}(OH)_2$	riebeck.1	Amphibole	Inosilicate
Tremolite	11	$Ca_2(MgFe)_5Si_8O_{22}(OH)_2$	tremol.1	Amphibole	Inosilicate
Biotite	12	$K(MgFe)_3(AlFe)Si_3O_{10}(OHF)_2$	biotite.1	Mica	Phyllosilicate
Muscovite	13	$KAl_2(Si_3Al)O_{10}(OHF)_2$	muscov.1	Mica	Phyllosilicate
Phlogopite	14	$KMg_3(Si_3Al)O_{10}(OHF)_2$	phlogop.1	Mica	Phyllosilicate
Labradorite	15	$(NaCa)Al(AlSi)Si_2O_8$	labrador.1	Feldspar	Tektosilicate
Microcline	16	$KAlSi_3O_8$	micro.1	Feldspar	Tektosilicate
Orthoclase	17	$KAlSi_3O_8$	orthocl.3	Feldspar	Tektosilicate
Sanidine	18	$(KNa)Al_3O_8$	sanidine.3	Feldspar	Tektosilicate
Leucite	19	$KAlSi_2O_6$	leucite.1	Feldspathoid	Tektosilicate
Nepheline	20	$(NaK)AlSiO_4$	nephel.2	Feldspathoid	Tektosilicate
Sodalite	21	$Na_4Al_3(SiO_4)_3Cl$	sodalite.1	Feldspathoid	Tektosilicate
Quartz	22	SiO_2	quartz.1	Silica	Tektosilicate
Almandine	23	$Fe_2Al_2(SiO_4)_3$	almandine.1	Garnet	Nesosilicate
Andradite	24	$Ca_3Fe_3(SiO_4)_3$	andradite.1	Garnet	Nesosilicate
Grossular	25	$Ca_3Al_2(Si0_4)_3$	grossul.2	Garnet	Nesosilicate
Pyrope	26	$Mg_3Al_2(SiO_4)_3$	pyrope.1	Garnet	Nesosilicate
Antigorite	27	$(MgFe)_3Si_2O_5(OH)_4$	antigorite.1	Serpentine	Phyllosilicate
Talc	28	$Mg_3Si_4O_{10}(OH)_2$	talc.1	Talc/Pyrophyllite	Phyllosilicate
Pyrophyllite	29	$Al_2Si_4O_{10}(OH)_2$	pyroph.1	Talc/Pyrophyllite	Phyllosilicate

[a]Mineral ID shown on Figs. 4, 6 and 7; [b] Filename appearing in the ENVI spectral library. Three spectra (solid, fine and coarse powders) were used for each mineral.

Table 3
List of minerals and filename of spectra selected from the USGS library

Mineral ID/Name	Spectral ID	USGS filename[a]	ENVI filename [b]	EM[c]
1/Dickite	1	Dickite NMNH106242	dickite1	
	2	Dickite NMNH46967	dickite2	X
2/Kaolinite	3	Kaolinite CM9	kaolini1	
	4–5	Kaolinite KGa-1; 2	kaolini2; kaolini3	X (kaolini 2)
	6	Kaolinite KL502	kaolini4	
	7	Kaolinite GDS11 <63 um	kaolini5	
	8	Kaolinite CM3	kaolini6	
	9	Kaolinite CM5	kaolini7	
	10	Kaolinite CM7	kaolini8	
3/Nacrite	11	Nacrite GDS88	Nacrite	X
4/Illite	12	Illite GDS4 (Marblehead)	illite1	
	13–14	Illite IMt-1.a; 1.b<2 μm	illite2; illite3	X (illite 2)
	15	Illite IL101 (2M2)	illite4	
	16	Illite IL105 (1Md)	illite5	
5/Montmorillonite	17	Montmorillonite SWy-1	montmor1	
	18	Montmorillonite SAz-1	montmor2	
	19–20	Montmorillonite SCa-2.a; 2.b	montmor3;montmor4	
	21	Montmorillonite CM27	montmor5	
	22	Montmorillonite CM20	montmor6	
	23	Montmorillonite CM26	montmor7	
	24	Montmorillonite STx-1	montmor8	X
6/Pyrophyllite	25	Pyrophyllite	pyrophy1	
	26	Pyrophyllite PYS1A<850 um	pyrophy2	X
	27	Pyrophyllite SU1421	pyrophy3	
7/Talc	28	Talc GDS23 74-250 um	talc1	
	29	Talc HS21.3B	talc2	
	30	Talc WS659	talc3	X
	31	Talc TL2702	talc4	
8/Vermiculite	32	Vermiculite GDS13 Llano	vermicu1	
	33	Vermiculite VTx-1.a<250	vermicu2	
	34	Vermiculite VTx-1.fls	vermicu3	
	35	Vermiculite WS681	vermicu4	
9/Sauconite	36	Sauconite GDS135	Sauconit	X
10/Saponite	37	Saponite SapCa-1	saponit1	
	38	Saponite SapCa-1.AcB	saponit2	X
11/Nontronite	39	Nontronite GDS41	nontron1	
	40–41	Nontronite NG-1.a; 1.b<2 μm	nontron2; nontron3	
	42	Nontronite SWa-1.a	nontron4	X
	43	Nontronite SWa-1.b<2 μm	nontron5	
12/Muscovite	44	Muscovite GDS107	muscovi1	
	45	Muscovite GDS108	muscovi2	
	46	Muscovite GDS111 Guatemal	muscovi3	
	47	Muscovite GDS113 Ruby	muscovi4	X
	48	Muscovite GDS114 Marshall	muscovi5	
	49	Muscovite GDS116 Tanzania	muscovi6	
	50	Muscovite GDS117 Isinglas	muscovi7	
	51	Muscovite GDS118 Capitan	muscovi8	
	52	Muscovite GDS119 Mt Alamo	muscovi9	
	53	Muscovite GDS120 Pegma M	muscovia	
	54	Muscovite HS146.3B	muscovib	
	55	Muscovite HS24.3	muscovic	
	56	Muscovite IL107	muscovid	

[a]See Clark et al. (1993) for sample description; [b]As appears in ENVI spectral library; [c]EM=endmember.

1993), geophysics (Kumar and Foufoula-Georgiou, 1997; Morlet et al., 1982; Grossmann & Morlet, 1984), medical science (Angelini et al., 2001; Dima et al., 2002; Dinov et al., 2002; Unser & Aldroubi, 1996) and multiscale image analysis (Porter & Canagarajah, 1996; Unser 1995; Weaver et al., 1991) to extract information from various scales. Recent studies (Bruce & Li, 2001; Bruce et al., 2001, 2002, 2006; Li & Bruce, 2004) have demonstrated the merits of using wavelet deconvolution for the analysis of hyperspectral data because such data exhibit non-stationarity, that is, spectral signals can vary in both amplitude (e.g. feature depth) and scale (e.g. feature width). Wavelet analysis can be implemented as a continuous wavelet transform (CWT) or a discrete wavelet transform (DWT). The use of the CWT rather than the DWT in this study is based on the consideration that outputs from the CWT (namely the power and significance spectra) are directly comparable to the original

spectrum and are more easily interpretable. We begin with a description of the method followed in Section 4 by an example result applied to a spectrum.

Our aim in using the CWT is to represent an original spectrum as a suite of spectra known as wavelets, each capturing spectral features of different widths here referred to as scales. In such a representation, narrow absorption features in the original spectrum will be captured by wavelets at a low scale (narrow width) while the shape of the continuum will be captured by wavelets at a higher scale. As a first step, the mean reflectance of the spectrum calculated over the entire spectral range is subtracted at each band. This mean subtraction is required to ensure that the wavelets are comparable between scales, and that the wavelets from different original spectra are comparable at the same scale. The original spectrum can be reconstructed by adding the mean back to the modified spectrum. To compute the wavelets, the original spectrum ($X_{n'}$,n' = spectral band 1,..., N) is convolved with a fixed-shape signal (a wavelet base, ψ) at various scales (S) to extract the spectral information:

$$W_n(s) = \sum_{n'=0}^{N-1} x_{n'} \psi \left[\frac{(n' - n)\delta t}{s} \right]$$

where N is the number of bands and δt is the minimum band interval. The input spectrum must contain a constant band interval. For this study, the shape of the wavelet base chosen is the 2nd order derivative of Gaussian (DOG, Muraki, 1995) as explained in the following section. By varying the wavelet scale S and translating the wavelet base (which acts like a filter) along the local band n, the convolution will decompose an original spectrum into various wavelet power (W) spectra at different scales. At any given scale, the amplitude of the wavelet base required to capture the amplitude of features in the original spectrum will be recorded as the power (W). For each wavelet scale, a significance spectrum can then be calculated (Torrence & Compo, 1998) based on how the local power spectrum (W) deviates from the mean. If a peak or trough on the wavelet power spectrum at each scale is significantly above or below the local mean at the current scale, it is considered significant. The significance can be set to different confidence levels (90% was used in this study). The significance spectrum at a given scale is determined by calculating the deviation (captured by 90% of the variation) of the power spectrum from its local mean. The significance spectrum at a set confidence level represents the relative strength of absorption features at a specific scale.

The peaks and troughs of reflectance spectra are shown as peaks and troughs on their wavelet power spectrum at the corresponding scale. However, they are all represented by peaks (features of higher significance) on the significance spectrum at the same scale.

3.2. Simplifications for the analysis of powdered mineral spectra

The spectral features contained within the spectral libraries listed in Table 1 span the visible, near infrared and thermal infrared spectrum (0.2–45.0 μm) and encompass a range of mineral electronic and vibrational processes (Burns, 1993; Salisbury et al., 1991). Within reflectance spectra, these processes give rise to absorption features or reflectance peaks depending on the spectral range of observation or physical properties of the sample. Individual spectral features can be represented by Gaussian or quasi-Gaussian functions. Torrence and Compo (1998) recommends that the shape of a wavelet base (ψ) reflect the property of features present in the original spectrum, thus we made use of the 2nd order derivative of Gaussian (DOG) as a base. DOG has a zero mean power, a mathematical prerequisite for the wavelet base used to perform the CWT on discrete data series such as spectral libraries. The DOG base captures positive and negative oscillations (e.g. peaks and troughs) of the spectrum as separate peaks and troughs in the wavelet power spectra. The DOG base provides sufficient resolution in wavelength for locating features and their inflection points. The latter are key to define the width of features.

For each of the experiments we computed ten wavelet scales from each original spectrum. Computing ten scales meant that we could capture features as wide as 1024 bands as discussed below, a conservative selection for mineral spectra. Mineral spectral features resulting from a given process (e.g. cation-OH vibrations in the near infrared) tend to be similar in width and thus occur within similar wavelet scales. Consequently it is possible to simplify the wavelet analysis of mineral spectra by adding the scales into two categories: low scale components of power (LCP) and its significance (LCS) containing mineral spectral features, and high scale components of power (HCP) and its significance (HCS) capturing the overall continuum. The high scale components have been used for baseline removal in chemometrics (Alsberg et al., 1997). For the first two experiments the reflectance spectra of the ASU and JPL libraries were resampled to the band location and 2 cm^{-1} band spacing of the JHL library. Given that the thermal infrared features of minerals are generally less than 32 bands in width (e.g. 0.4–0.7 μm at 10 μm), a summation of wavelet power spectra at $S \leq 5$ captures narrow features and forms the LCP spectrum. This is because at

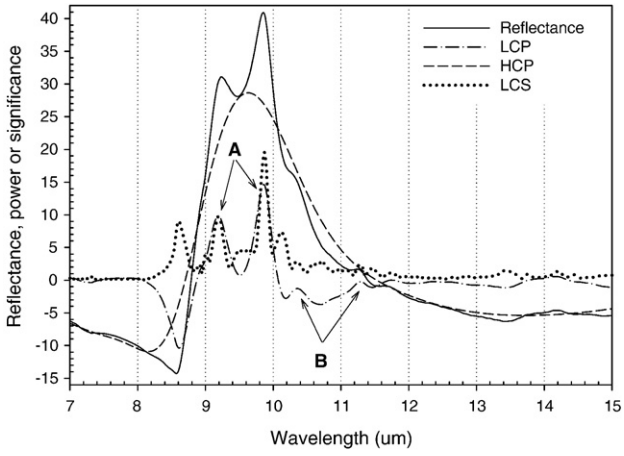

Fig. 1. Reflectance spectrum (shifted to zero mean) and wavelet power and significance spectra of solid biotite [$K(MgFe)_3(AlFe)Si_3O_{10}(OHF)_2$]. The reflectance spectrum (Table 2, sample Biotite.1) is from the John Hopkins University spectral library. Strong features are marked by A and weak features by B.

any wavelet scale, the maximum feature width given in number of bands is equal to 2^S (e.g. 32 bands at scale $s=5$). Wavelet spectra at higher scales ($S>5$) are summed and form the HCP spectrum.

4. Results

4.1. Illustration of wavelet results

To familiarize readers with the various components of wavelet analysis, wavelet results for a sample of the mineral biotite are shown in Fig. 1. From this figure we can outline five general properties of wavelet spectra:

(a) The HCP spectrum captures properties of the continuum and retains the overall shape and amplitude of the original reflectance spectrum, which, as shown below, relate to non-compositional factors (target physical properties, illumination geometry, etc). (b) The width and position of narrow spectral features are captured in the LCP spectrum and feature identification is considerably facilitated in the LCP spectrum compared to the original reflectance. (c) Features in LCP (peaks and troughs) are all peaks in LCS. (d) The relative strength of features in reflectance is preserved in the LCP spectra. (e) Local minima in LCS correspond to an inflection point in the LCP.

4.2. Experiment 1: minimizing spectral variance between libraries

We examined qualitatively if the spectral differences introduced by the disparities in sample grain size and in measurement methodologies amongst spectral libraries could be minimized. Fig. 2a displays spectra of the mineral quartz for a solid surface and a suite of powders from three different libraries. Quartz displays a doublet reflectance peak near 8.5 and 9.0 μm (Hunt & Salisbury, 1974; Ramsey & Christensen, 1998; Salisbury et al., 1991).

If the samples had been measured in a common viewing and illumination configuration one would expect a decrease in reflectance and feature strength of the quartz features with decreasing particle size but that is not observed (Fig. 2a). This is a spectral behavior observed for silicate minerals in the thermal infrared and is distinct from what is observed in the visible and near infrared. The strength of the 9.0 μm quartz feature (difference between 9.0 μm and 8.62 μm) ranges from 0.05 for the JHU-C (coarse grain, 75–250 μm grains) spectrum to 0.26

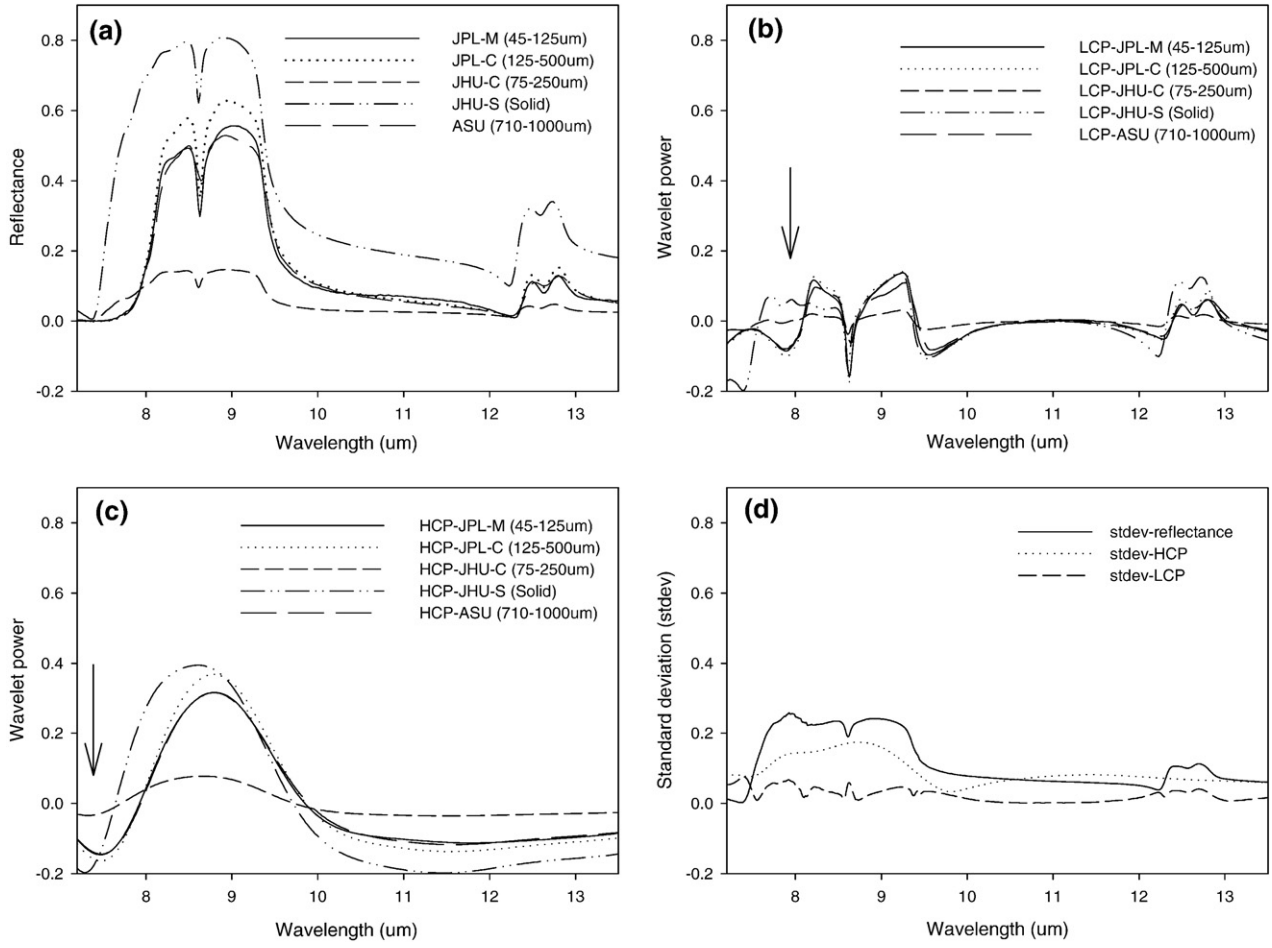

Fig. 2. Quartz spectra from the JPL, ASU and JHU libraries. (a) Reflectance; grain size: M = medium; C = coarse, S = solid; (b) LCP; arrows indicate spectral feature unique to the JHU samples; (c) HCP; arrow indicates the approximate locations of the Christensen Frequency for the JPL and ASU samples; (d) standard deviation for the five spectra.

for the JPL-M (medium grain, 45–125 μm grains) spectrum. The standard deviation of the five spectra from the JPL, ASU and JHU libraries (Fig. 2d) for this feature is similar for the reflectance (0.24) and HCP (0.15) and much reduced for the LCP (0.04) in accordance with the increased similarity in shape and amplitude of all spectra in LCP (Fig. 2b). These qualitative observations suggest that the variability in reflectance observed for spectral features of mineral powders of varying grain size can be largely captured in HCP (Fig. 2c) and minimized in LCP.

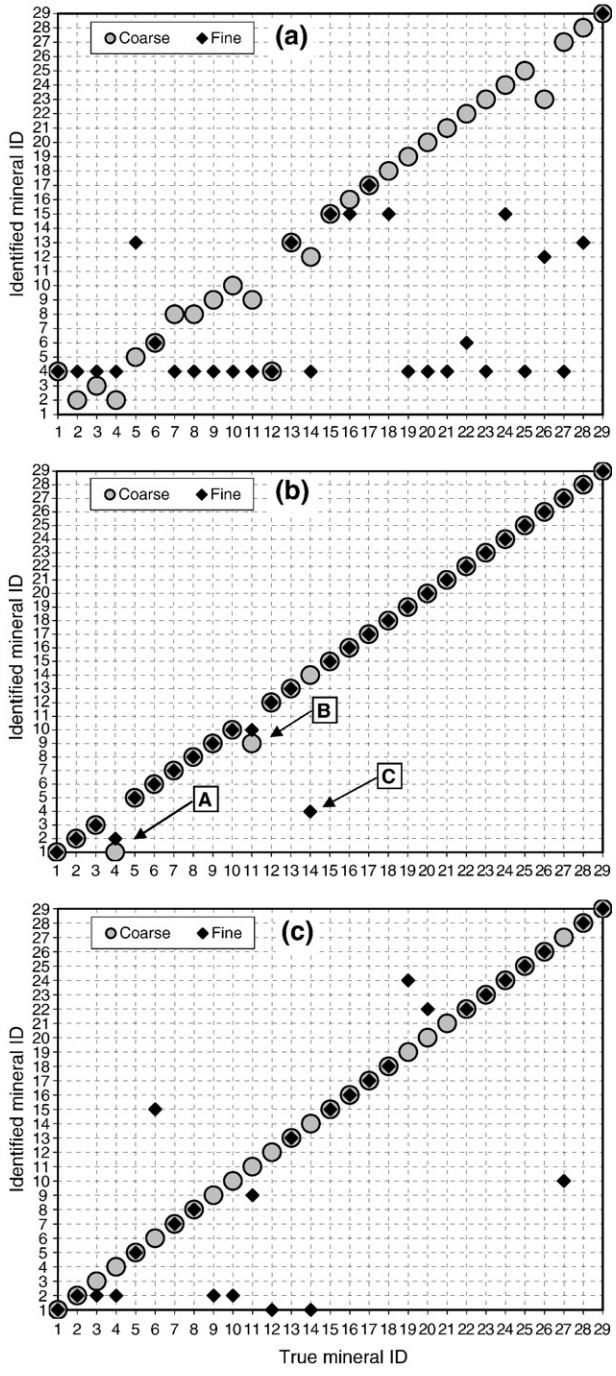

Fig. 3. Mineral identification results using spectra of solid samples as endmember inputs to SAM. (a) reflectance; (b) LCP spectra, Hypersthene (A, ID=4), Tremolite (B, ID=11) and Phlogopite (C, ID=14); and (c) LCS. Mineral ID listed in Table 2. The spectral angle was computed for the 7.4–13.3 um spectral region (750–1350 cm^{-1}).

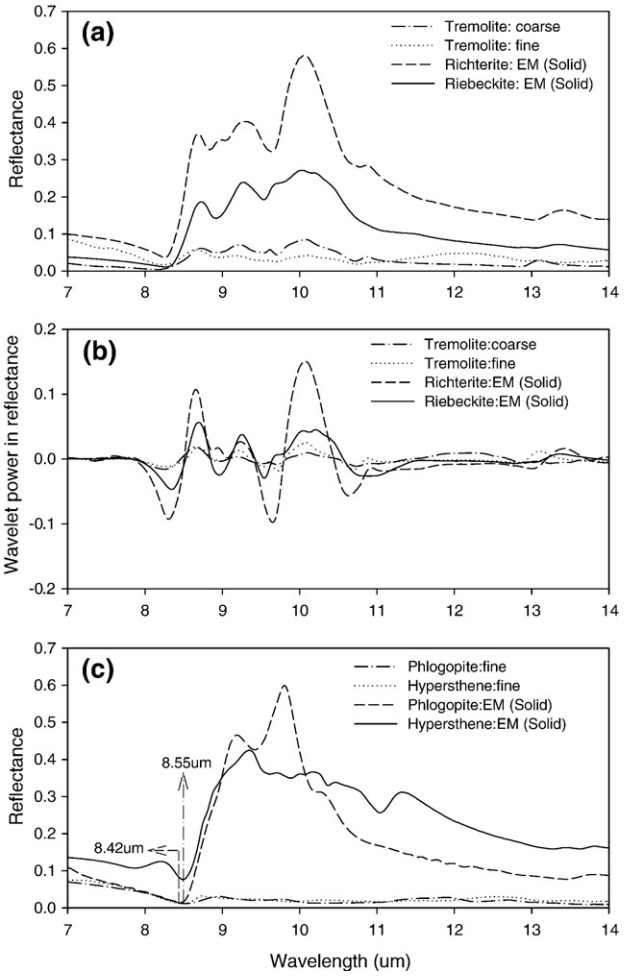

Fig. 4. Spectra of most confused minerals. (a) Richterite, riebeckite endmembers and tremolite spectra from coarse and fine particles; (b) Respective LCP spectra; (c) Solid and fine-grained phlogopite and hyperthene reflectance spectra with Christensen Frequency locations marked by arrows.

The LCP spectra reveal that both samples from the JHU library display additional features near 7.5 μm (Fig. 2b) and a shorter wavelength location of their Christensen frequency (wavelength of reflectance minima, Fig. 2c). These disparities with respect to the ASU and JPL measurements are difficult to detect in the reflectance spectra and are likely due to compositional differences (e.g. sample impurities) of the JHU quartz samples.

4.3. Experiment 2: minimizing spectral effects of grain size

In a second experiment we examined quantitatively if the spectral effects introduced by only the variable grain size properties of 29 minerals can be minimized using wavelets. We focused on a subset of the JHU library encompassing 29 minerals (Table 2) and 87 spectra (29 * 3) at varying grain size (fine, coarse and solid).

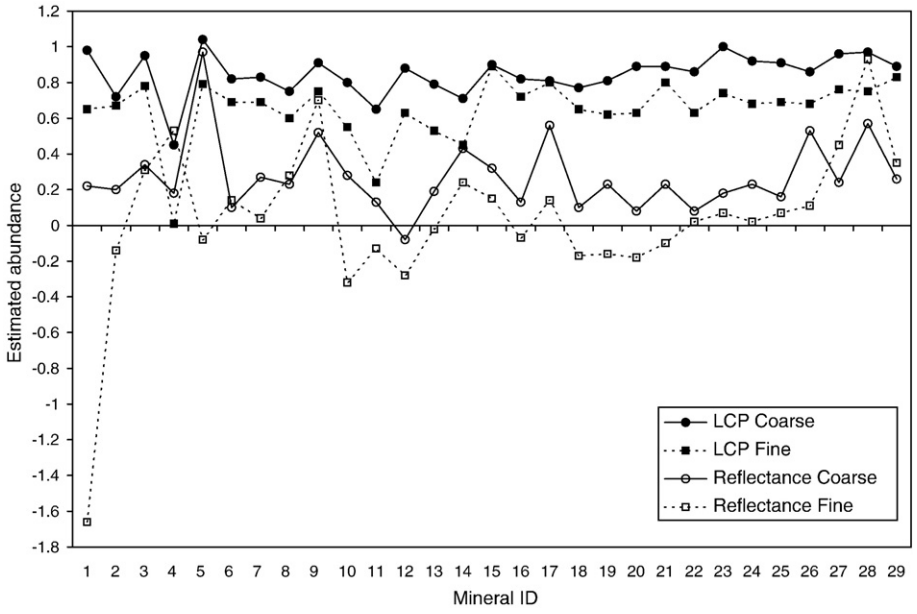

Fig. 5. Mineral endmember ID abundances estimated from the unconstrained linear spectral unmixing (LSU) for the powders of the same mineral ID. For example for ID5, we show the abundance of mineral ID5 when unmixing the coarse and fine powders of mineral ID5. Spectra of the 29 solid samples were used as endmember for linear unmixing. See Table 2 for mineral ID.

4.3.1. Spectral angle mapper

For each mineral we began by comparing the spectrum of the solid sample to the remaining 86 spectra. We found the spectra for a coarse and a fine grain sample with the smallest spectral angle to the spectrum of the solid surface. We did so by treating each spectrum as a vector and computed the angle between vector pairs using the spectral angle mapper (SAM). The experiment was repeated using reflectance, LCP and LCS since the first experiment indicated that the spectral variance within a given class (e.g. quartz) could be reduced using the LCP. Ideally,

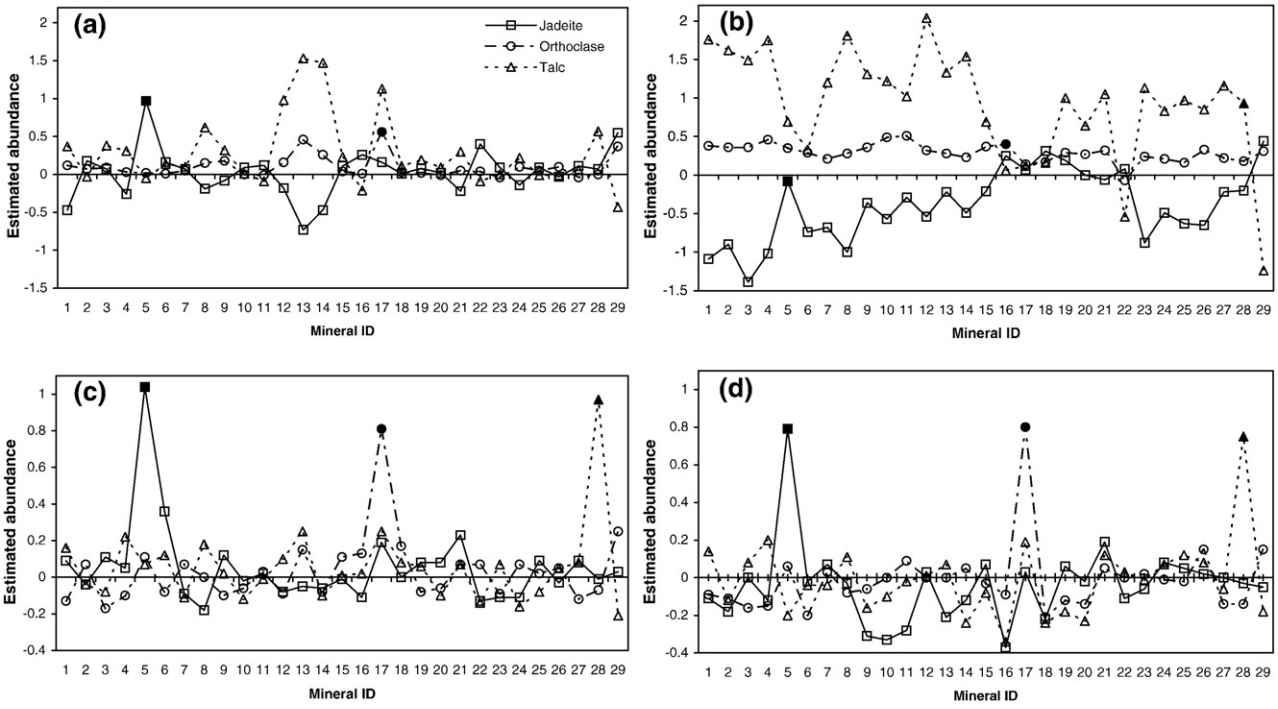

Fig. 6. Abundances of jadeite, orthoclase, and talc calculated for the coarse powder spectra of the 29 minerals (a), and for the fine powders (b). Abundances calculated for these minerals from the LCP are shown in (c) for coarse powders, and in (d) for fine powders. Mineral ID shown in Table 2. Filled square, diamond, and star symbols respectively mark the *x*-axis ID of jadeite, orthoclase and talc.

the spectra of the fine and coarse powder of a given mineral would show the smallest spectral angle with the spectrum of the solid surface for the same mineral and the spectral angle mapping accuracy would be 100% for all minerals. In addition we expected the highest accuracy would be observed for the analysis of the LCP.

Fig. 3 displays the mineral ID (Table 2) identified for the spectrum of each fine and coarse grain mineral powder. When the analysis is conducted using reflectance (Fig. 3a), the mineral ID accuracy is 75.9% for coarse grain samples and 17.2% for fine grain samples. The fine grain samples display high errors because their spectra display features with low contrast. The accuracy for the LCP data (Fig. 3b) is considerably improved for the coarse grain (93.1%) and fine grain (89.7%) samples. The improvement for the fine grain samples is dramatic and the difference in accuracy for both grain sizes is small compared to that observed for the reflectance data suggesting that grain size difference can be minimized in LCP.

The misidentifications in LCP are observed for 3 minerals namely hypersthene (ID=4), tremolite (ID=11) and phlogopite (ID=14) (labels ABC on Fig. 3b). Hypersthene is misidentified as augite and enstatite, which belong to the same mineral group (pyroxene group). Tremolite is misidentified with two other amphibole minerals (richterite and riebeckite). For minerals belonging to the same group, the spectra of samples can be very similar as illustrated in Fig. 4a,b for tremolite, richterite and riebeckite. The strongest spectral features of these minerals are observed at the same wavelengths and the use of LCP only enhances weak discriminating features that do not substantially influence the SAM results given the broad spectral range (7.4–13.3 μm) over which the analysis is conducted. The fine grain phlogopite sample was classified as hypersthene. The thermal infrared reflectance of fine grain mineral samples can be very low with low contrast as observed for hypersthene and phlogopite (<2.7%, Fig. 4c). The most distinctive feature of the fine grain phlogopite spectrum is the Christensen Frequency (CF) feature located at 8.42 μm that appears to be confused with that of hypersthene at 8.55 μm. The low spectral contrast of fine grain samples explains the lower accuracy obtained with the LCS (62.07%) as opposed to the LCP (89.66%) (Fig. 3b,c). As illustrated in Section 4.1 the relative strength of features in reflectance is linearly preserved in the LCP spectra but not in the LCS spectra (Fig. 1) thus because fine powders have low contrast their LCS spectra are somewhat more confused than their respective LCP spectra. For coarse grain samples however, the accuracy is 100% in LCS.

4.3.2. Linear spectral unmixing

Using the same spectral data we then examined the abundances estimated for each coarse and fine grained powder spectra. For this purpose the spectra of the 29 mineral solid surfaces were used as endmember inputs for an unconstrained linear spectral unmixing solution. In essence we pretended that the spectra of the mineral powders were mixtures and examined: 1) whether the highest predicted abundances were observed for the endmember of the same mineral, 2) whether the abundances were close to 1 (e.g. 100% and a match), and 3) whether confusion arose with other minerals. Results were compared for reflectance and LCP, with the hypothesis that the analysis using LCP wavelets would yield abundances closer to 1 for coarse and fine powders than reflectance spectra would. Given the broad use of linear spectral unmixing for the analysis of hyperspectral imagery, this analysis could provide valuable insights to minimize errors in unmixing solutions introduced by variability in grain size of mixtures and spectral endmembers.

Generally the endmember abundance estimated for the fine and coarse powders of the same mineral using wavelet LCP were closer to 1.0 (average of 0.70 for fine and 0.87 for coarse powders) and less variable than abundances obtained from reflectance spectra (average of 0.04 for fine and 0.27 for coarse powders) (Fig. 5). Abundances are higher when estimated from LCP rather than reflectance for 25 of the 29 samples. We interpret these results to indicate that the variability in the reflectance amplitude of the continuum with grain size causes inaccurate abundance estimations. Because the LCP spectra display much lower amplitude variability, the solution then depends on the location and strength of spectral features and these tend to be similar for the same mineral. The fine grain hypersthene (ID=4) is an exception,

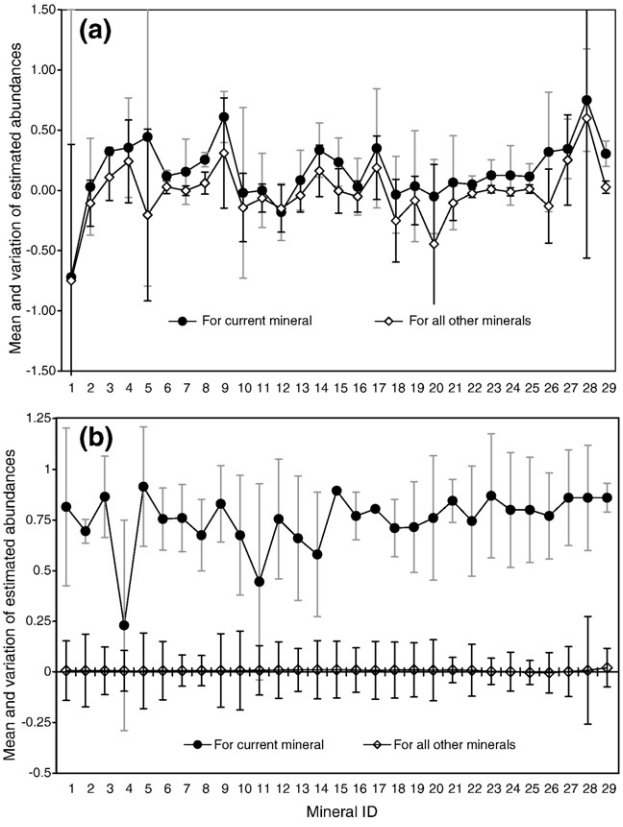

Fig. 7. Mean (coarse and fine together) of the LSU abundance solution for the given mineral endmember (filled circle) and all other minerals endmembers (diamonds) of the same unmixing solution. For example, the filled circle for mineral 2 enstatite is the mean abundance of the enstatite endmember when the spectra of the coarse and fine enstatite powder are analyzed, and the open diamond is the mean abundance of all 28 other endmembers when the spectra of the enstatite powders are analyzed: (a) abundances estimated from reflectance; (b) abundances estimated from the LCP. The error bar are ±1.67×standard deviation of the means to approximate a 95% confidence limit.

it shows very low abundances for LCP (Fig. 5) likely due to the very low reflectance and lack of spectral features as discussed in the previous section.

Fig. 6 shows the abundances of jadeite, orthoclase, and talc predicted by unmixing the powder spectra of the 29 minerals. The coarse powders of these three minerals showed the highest abundances of these minerals when estimated from reflectance (Fig. 5: open circles, jadeite ID5, orthoclase ID17, and talc ID28). To clarify, the results in Figs. 5 and 6 are from the same linear unmixing analysis. Fig. 5 presents results for 29 samples (coarse and fine), displaying the abundance result for only the mineral endmember matching the mineral ID of the powder (e.g. ednmember 5 for unmixing powder of mineral ID5). Fig. 6 presents the abundances of three minerals predicted when unmixing powders of all 29 minerals. One would expect high abundances for these three minerals when unmixing powders of these same minerals and low abundances for all other minerals. However, the abundances estimated from the reflectance data are highly variable for all three minerals (Fig. 6a,b) with multiple powders of other minerals ID's showcasing abundances in excess of 0.5 for all three minerals. With the exception of the coarse jadeite powder the highest abundance is predicted for another mineral. It would therefore be misleading to label the mineral powder based on the endmember with highest abundance. This a commonly used operation and it would lead to misclassification. The problem is particularly evident for the fine powders (Fig. 6b). In contrast, the use of LCP leads to estimates that uniquely assign the highest abundance of a given mineral to the correct mineral powder spectra (e.g. >0.8 for each of the three minerals) (Fig. 6c,d). Abundances of these three minerals estimated for powders of other minerals do not exceed 0.2. This observation applies to fine and coarse powders and implies that errors in classification would be greatly reduced irrespective of grain size. The results observed for jadeite, orthoclase, and talc can be generalized to the 29 minerals investigated (Fig. 7). For every mineral the estimates obtained using the LCP show highest values for the correct mineral and the mean abundance of all other minerals is close to 0%. (Fig. 7b), a great improvement over results obtained from reflectance (Fig. 7a).

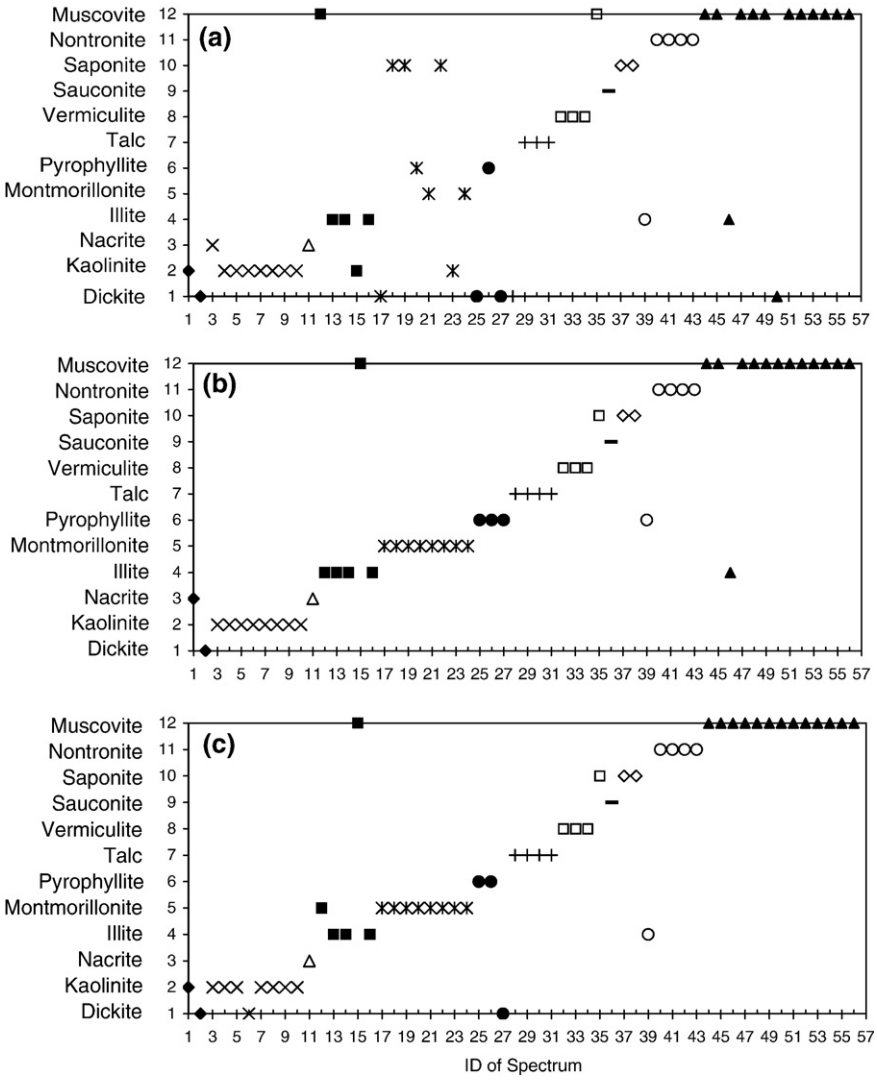

Fig. 8. Mineral identification results of SAM from 56 USGS spectra of 12 minerals from 0.45–2.5 μm: (a) reflectance; (b) LCS; and (c) LCP.

4.4. Experiment 3: discriminating clay minerals of the USGS library

For the last experiment we examined spectra of all clay mineral samples within the USGS library (56 spectra in Table 3). For each mineral we selected the spectrum with highest reflectance, typically that of a solid surface or coarse grain powder, and used it as the endmember against which all other spectra were compared in reflectance, in LCP and LCS. Spectra were compared and classified using SAM. The spectral resolution of the data varied from 2 nm in the visible to 32 nm in the near infrared. Thus the spectra were resampled to 4 nm to reduce noise in the visible and permit the computation of wavelets from 0.39–2.56 μm. In this region most of the iron absorption features are less than 230 nm in width (58 bands) and OH features are less than 75 nm in width (19 bands). A summation of wavelets power spectra for scales 1–6 (LCP) best extracts the absorption features less than 64 bands in width.

Fig. 8 displays the mineral identified for the 56 clay mineral spectra. When the analysis is conducted using reflectance (Fig. 8a), the mineral identification accuracy is 68% but it increases to 89% (LCS) and 84% (LCP) using wavelets (Fig. 8b,c). If the SAM comparison is conducted for the 2.0–2.5 μm region, a common practice for mineral exploration, the mineral identification accuracy improves marginally for the reflectance data (70%) but remains substantially lower than that observed from wavelets (LCP 84%, LCS 82%). The accuracy values are based on the results for the 44 non-endmember samples only (e.g. excluding the 12 endmember samples). Only one spectrum is available for nacrite and sauconite. Since this is used as the endmember representing the mineral, these two minerals do not affect the accuracy assessment. However their inclusion as endmembers in the SAM analysis does increase the possibility of misidentification.

The kaolinite, montmorillonite, pyrophylite and talc spectra were properly identified in the LCS wavelet domain (Fig. 8b) despite the varied geographical origin of the samples (Table 3) and thus potential compositional variability. Five spectra were not correctly identified using LCS namely Dickite1, Illite4, Vermiculite4, Nontronite1, and Muscovite3. In each case the spectra are distinct from other spectra of the same mineral (Fig. 9) likely caused by the distinct composition for these samples. Dickite1 is misidentified as kaolinite (LCS) (Fig. 8b) and nacrite (LCP) (Fig. 8c). X-ray Diffraction data shows that this sample is polymorphous and mixed with the mineral halloysite, kaolinite and nacrite. The Nontronite1 spectrum displays stronger iron absorptions features near 0.7–1 μm than the spectrum of the group mean (Fig. 9b), and the X-ray Fluorescence data reveals that this sample has 35.5% Fe_2O_3+MgO that is significantly higher than the other samples (average <20%). The Muscovite3 spectrum was measured from a sample with the highest Fe_2O_3 content (7.2%) of its group (average <3.6%, largest 6.46%).

This experiment suggests that the spectral similarity of samples of a given mineral is best examined in the wavelet domain. These results are significant in two ways: 1) if spectra from mineral samples with similar compositional properties are available then representative mineral spectra can be more readily defined in the wavelet domain rather than using reflectance data, and 2) spectral differences due to distinct sample composition are more readily identified using the low component wavelets. The first point is relevant to spectral mixture analysis and to the selection of representative endmember spectra from spectral libraries. The second point is relevant to the detection of target compositional variability, for example changes in the chemistry of a given mineral.

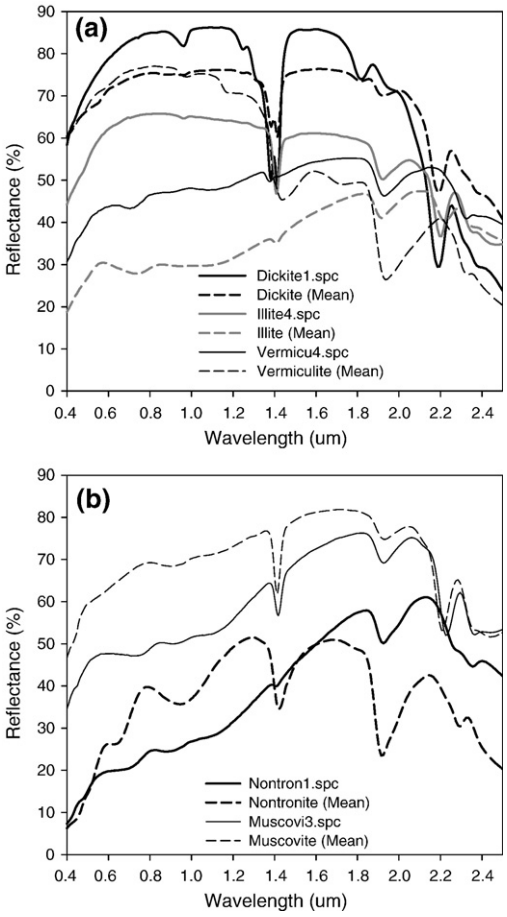

Fig. 9. Misidentified spectra and the mean of other spectra within their mineral group.

5. Discussion

5.1. Minimization of grain size effects

Variations in grain size impact both the amplitude of the continuum and the depth of spectral features. In the thermal infrared, feature strength decreases as grain size decreases (Clark & Roush, 1984; Hapke, 1993). Results from experiment 2 (Fig. 3) indicate that SAM matching accuracy can vary greatly as a function of grain size if one uses reflectance data. The spectra of coarse powders is characterized by higher amplitudes of the continuum and of the features compared to that of fine powders. For the fine powders, the weaker contrast of features with respect to the continuum implies a stronger impact of the shape of the continuum on the SAM results. That impact is minimized by the

use of LCP wavelets for which the matching accuracy is substantially improved (Fig. 3b). The unmixing results are also influenced by variations in the amplitude of the continuum attributed to grain size variations. Abundances computed from the reflectance data are generally lower for the fine grain size powders and in substantial error (Fig. 5). With the use of LCP, and thus minimization of the continuum component, the abundance errors are greatly minimized. However, the abundances computed for the fine grain powders are systematically lower than that of the coarser grain powders as one would expect given the weaker feature strength inherent to the finer materials.

5.2. Selection of scales

For the analysis of mineral spectra encompassed by the JPL, JHU, and ASU libraries, we chose to generate the LCP spectra from scales $S \leq 5$(Section 3.2). Our selection was dictated by the spectral resolution of the data that controls the number of possible scales, and by the width of features of interests. For the detection of features in clay minerals encompassed by the USGS library the LCP spectra were generated from scales $S < 7$. Thus to apply such CWT wavelet analysis to other materials we recommend an insightful selection of wavelet scales sensitive to target features which requires pre-existing knowledge of feature width.

5.3. HCP and HCS

The HCP and HCS wavelets were not extensively discussed because we aimed to highlight key spectral features, best shown in LCP and LCS spectra, to maximize the discrimination of minerals. However, the HCP and HCS wavelets may have value for other applications. For instance, in circumstances where the instrument setup has remained constant for all measurements and the variation of target physical properties is minimal, HCP may contain useful information to discern broad spectral classes. We are currently examining its use to guide a hierarchical rock type classification for rock cores extracted from boreholes. HCP may also have value for the investigation of target physical properties.

6. Conclusions

This study demonstrates that continuous wavelet analysis can provide a new and useful representation of spectral libraries. Disparities in measurement methodologies between libraries, and in variable mineral sample grain size between and within libraries, can be minimized with the use of LC wavelets. In the context of spectral mixture analysis we suggest that the selection of representative endmember spectra from spectral libraries can be more readily defined in the wavelet domain than using reflectance data. In the context of sensing target compositional variability, for example changes in the chemistry of a given mineral, spectral differences due to distinct sample composition are more readily identified using the low component wavelets. For target classification we suggest that errors in classification, in this case illustrated with unmixing, are greatly reduced irrespective of mineral grain size. Lastly because wavelets are linearly additive, linear spectral unmixing can be conducted in the wavelet domain.

Acknowledgements

Support from the GEOmatics for Informed Decisions (Geoide) Network of Centres of Excellence of Canada is gratefully acknowledged.

References

Adams, J. B., & Filice, A. L. (1967). Spectral reflectance of 0.4 to 2.0 mm of silicate rock powders. *Journal of Geophysical Research*, *72*, 5705−5717.

Alsberg, B. K., Woodward, A. M., & Kell, D. B. (1997). An introduction to wavelet transforms for chemometricians: A time-frequency approach. *Chemometrics and intelligent laboratory systems*, *37*, 215−239.

Angelini, E., Laine, A., Takuma, S., Holmes, J., & Homma, S. (2001). LV volume quantification via spatio-temporal analysis of real-time 3D echocardiography. *IEEE Transactions on Medical Imaging*, *20*, 457−469.

Bruce, L. M., & Li, J. (2001). Wavelets for computationally efficient hyperspectral derivative analysis. *IEEE Transactions on Geoscience and Remote Sensing*, *39*(7), 1540−1546.

Bruce, L. M., Li, J., & Huang, Y. (2002). Automated detection of subpixel hyperspectral targets with adaptive multichannel discrete wavelet transform. *IEEE Transactions on Geoscience and Remote Sensing*, *40*(4), 977−979.

Bruce, L. M., Mathur, A., & Byrd, J. D. (2006). Denoising and wavelet-based feature extraction of MODIS multi-temporal vegetation signatures. *GIScience & Remote Sensing*, *43*, 170−180.

Bruce, L. M., Morgan, C., & Larsen, S. (2001). Automated detection of subpixel targets with continuous and discrete wavelet transforms. *IEEE Transactions on Geoscience and Remote Sensing*, *39*(10), 2217−2226.

Burns, R. (1993). *Mineralogical Applications of Crystal Field Theory*, Second Edition Cambridge: Cambridge University Press 551 pp.

Christensen, P. R., Bandfield, J. L., Hamilton, V. E., Howard, D. A., Lane, M. D., Piatek, J. L., et al. (2000). A thermal emission spectral library of rock forming minerals. *Journal of Geophysical Research*, *105*, 9735−9739.

Clark, R. N. (1999). Chapter 1: Spectroscopy of rocks and minerals, and principles of spectroscopy. In A. N. Rencz (Ed.), *Manual of Remote SensingRemote Sensing for the Earth Sciences*, *vol. 3*. (pp. 3−58) New York: John Wiley and Sons.

Clark, R. N., Gallagher, A. J., & Swayze, G. A. (1990). Material absorption band depth mapping of imaging spectrometer data using the complete band shape least-squares algorithm simultaneously fit to multiple spectral features from multiple materials. *Proceedings of the Third Airborne Visible/Infrared Imaging Spectrometer (AVIRIS) Workshop*, *vol. (90–54)*. (pp. 176−186): JPL Publication.

Clark, R. N., & Roush, T. L. (1984). Reflectance spectroscopy: Quantitative analysis techniques for remote sensing applications. *Journal of Geophysical Research*, *89*, 6329−6340.

Clark, R. N., & Swayze, G. A. (1995). Mapping minerals, amorphous materials, environmental materials, vegetation, water, ice, and snow, and other materials: The USGS tricorder algorithm. *Summaries of the Fifth Annual JPL Airborne Earth Science Workshop*, *vol. 95–1*. (pp. 39−40): JPL Publication.

Clark, R. N., Swayze, G. A., Gallagher, A. J., King, T. V., & Calvin, W. M. (1993). *The U.S. Geological Survey digital spectral library: Version 1: 0.2 to 3.0 micronsOpen File Report*, *vol. 93–592*. U.S. Geological Survey 1340 pp.

Clark, R. N., Swayze, G. A., Livo, K. E., Kokaly, R. F., Sutley, S. J., Dalton, J. B., et al. (2003). Imaging spectroscopy: Earth and planetary remote sensing with the USGS tetracorder and expert systems. *Journal of Geophysical Research*, *108*(E12), 5133−5177.

Conel, J. E. (1969). Infrared emissivities of silicates: Experimental results and a cloudy atmosphere model of spectral emission from condensed particulate mediums. *Journal of Geophysical Research*, *74*, 1614−1634.

Dima, A., Scholz, M., & Obermayer, K. (2002). Automatic segmentation and skeletonization of neurons from confocal microscopy images based on the 3-D wavelet transform. *IEEE Transactions on Image Processing*, *11*(7), 790−801.

Dinov, I., Mega, M., Thompson, P., Woods, R., Sumners, D., Sowell, E., et al. (2002). Quantitative comparison and analysis of brain image registration using frequency-adaptive wavelet shrinkage. *IEEE Transactions on Information Technology in Biomedicine*, *6*(1), 73−85.

Farge, M. (1992). Wavelet transforms and their applications to turbulence. *Annual Review of Fluid mechanics*, *24*, 395−457.

Grossmann, A., & Morlet, J. (1984). Decomposition of Hardy functions into square integrable wavelets of constant shape. *SIAM Journal on Mathematical Analysis*, *15*(4), 723−736.

Grove, C. I., Hook, S., & Paylor, E. (1992). Laboratory reflectance spectra of 160 minerals, 0.4 to 2.5 micrometers. *JPL Publication 92–2, Pilot land data system* Pasadena, California: Jet Propulsion laboratory 405 pp.

Hapke, B. (1981). Bidirectional reflectance spectroscopy, 1, theory. *Journal of Geophysical Research*, *86*, 3039−3054.

Hapke, B. (1993). *Introduction to the Theory of reflectance and Emittance Spectroscopy.* New York: Cambridge University Press 455 pp.

Hunt, G. R., & Salisbury, J. W. (1974). *Mid-infrared spectral behavior of igneous rocks: Environmental Research Paper 496-AFCRL-TR-74-0625, Hanscom Air Force Base.* U.S.A: Air Force Cambridge Research Laboratories 142 pp.

Johnson, P. E., Smith, M. O., & Adams, J. B. (1992). Simple algorithms for remote determination of mineral abundances and particle sizes from reflectance spectra. *Journal of Geophysical Research*, *97*(E2), 2649−2657.

Johnson, P. E., Smith, M. O., Taylor-George, S., & Adams, J. B. (1983). A semiemperical method for analysis of the reflectance spectra of binary mixtures. *Journal of Geophysical Research*, *88*, 3557−3561.

Kruse, F. A., Lefkoff, A. B., Boardman, J. B., Heidebrecht, K. B., Shapiro, A. T., Barloon, P. J., et al. (1993). The spectral image processing system (SIPS) — Interactive visualization and analysis of imaging spectrometer data. *Remote Sensing of the Environment*, *44*, 145−163.

Kumar, P., & Foufoula-Georgiou, E. (1997). Wavelet analysis for geophysical applications. *Reviews of Geophysics*, *35*(4), 385−412.

Li, J., & Bruce, L. M. (2004). Wavelet-based feature extraction for improved endmember abundance estimation in linear unmixing of hyperspectral signals. *IEEE Transactions on Geoscience and Remote Sensing*, *42*(3), 644−649.

Meyers, S. D., Kelly, B. G., & O'Brien, J. J. (1993). An introduction to wavelet analysis in oceanography and meteorology: With application to the dispersion of Yanai waves. *Monthly Weather Review*, *121*(10), 2858−2866.

Morlet, J., Arens, G., Fourgeau, E., & Glard, D. (1982). Wave propagation and sampling theory, 1, complex signal and scattering in multilayered media. *Geophysics*, *47*(2), 203−221.

Muraki, S. (1995). Multiscale volume representation by a DOG wavelet. *IEEE Transactions on visualization and computer graphics*, *1*(2), 109−116.

Mustard, J. F. (1992). Chemical analysis of actinolite from reflectance spectra. *American Mineralogist*, *77*, 345−358.

Mustard, J. F., & Hayes, J. E. (1997). Effects of hyperfine particles on reflectance spectra from 0.3 to 25 μm. *Icarus*, *125*, 145−163.

Mustard, J. F., & Pieters, C. M. (1989). Photometric phase functions of common geologic minerals and applications to quantitative analysis of mineral mixture reflectance spectra. *Journal of Geophysical Research*, *94*(B10), 13,619−13,634.

Mustard, J., & Sunshine, J. (1999). Chapter 5: Spectral analysis for earth science investigation. In A. N. Rencz (Ed.), *Manual of Remote Sensing, Remote Sensing for the Earth Sciences*, *vol. 3*. (pp. 3−58) New York: John Wiley and Sons.

Pieters, C. M. (1983). Strength of mineral absorption features in the transmitted component of near-infrared reflected light — First results from RELAB. *Journal of Geophysical Research*, *88*, 9534−9544.

Porter, R., & Canagarajah, N. (1996). A robust automatic clustering scheme for image segmentation using wavelets. *IEEE Transactions on Image Processing*, *5*(4), 662−665.

Ramsey, M. S., & Christensen, P. R. (1998). Mineral abundance determination: Quantitative deconvolution of thermal emission spectra. *Journal of Geophysical Research*, *103*, 577−596.

Ruff, S. W., Christensen, P. R., Barbera, P. W., & Anderson, D. L. (1997). Quantitative thermal emission spectroscopy of minerals: A laboratory technique for measurement and calibration. *Journal of Geophysical Research*, *102*, 14,899−14,913.

Salisbury, J. W., Wald, A., & D'Aria, D. M. (1994). Thermal-infrared remote sensing and Kirchhoff's law 1. Laboratory measurements. *Journal of Geophysical Research*, *99*(B6), 11897−11911.

Salisbury, J. W., Walter, L. S., Vergo, N., & D'Aria, D. M. (1991). *Infrared (2.1–25 μm) spectra of minerals.* Baltimore: The Johns Hopkins University Press 267 pp.

Sunshine, J. M., & Pieters, C. M. (1993). Estimating modal abundances from the spectra of natural and laboratory pyroxene mixtures using the modified Gaussian model. *Journal of Geophysical Research*, *98*, 9075−9087.

Sunshine, J. M., Pieters, C. M., & Pratt, S. F. (1990). Deconvolution of mineral absorption bands: An improved approach. *Journal of Geophysical Research*, *95*(B5), 6955−6966.

Swayze, G. A., & Clark, R. N. (1995). Spectral identification of minerals using imaging spectrometry data: evaluating the effects of signal to noise and spectral resolution using the Tricorder Algorithm. *Summaries of the Fifth Annual JPL Airborne Earth Science Workshop*, *vol. 95–1*. (pp. 157−158): JPL Publication.

Torrence, C., & Compo, G. P. (1998). A practical guide to wavelet analysis. *Bulletin of the American Meteorological Society*, *79*, 61−78.

Unser, M. (1995). Texture classification and segmentation using wavelet frames. *IEEE Transactions on Image Processing*, *4*(11), 1549−1560.

Unser, M., & Aldroubi, A. (1996). A review of wavelets in biomedical applications. *Proceedings IEEE*, *84*(4), 626−638.

Weaver, J. B., Yansun, X., Healy, D. M., & Cromwell, L. D. (1991). Filtering noise from images with wavelet transforms. *Magnetic Resonance in Medicine*, *21*(2), 288−295.